

# Bilevel Image Degradations: Effects and Estimation

Elisa H. Barney Smith

EBarneySmith@boisestate.edu

Electrical and Computer Engineering Department

Boise State University, Boise, Idaho 83725, USA

Phone: 208-426-2214

## Abstract

The two most significant parameters affecting degradations of bilevel images are the point spread function (PSF) width and the binarization threshold. Each pair of these values will affect an image differently. However, several combinations of these parameters will affect images in a similar fashion. This paper looks at two aspects of image degradation: the displacement of an edge, which determines stroke width, and the erosion of a corner, which affects crispness. The relationship between the PSF width and the binarization threshold and these two effects will be described. Sample characters, first with similar edge displacement and second with similar corner erosion, will show the effect of estimating the broader degradation versus the exact system parameters. Methods of estimating these degradations will also be briefly discussed.

## 1. Introduction

Bilevel processes such as scanning, photocopying, faxing, and printing cause many degradations to document images. These processes are characterized by spatial and intensity quantization, which changes the appearance of the image content, such as characters and line drawings. The ability to characterize the degradations that are introduced when a document passes through a bilevel process is an important step toward improving recognition accuracy. This paper discusses bilevel degradations in the context of the scanning process.

Baird developed a degradation model that contained 10 parameters: resolution, blur, threshold, sensitivity, jitter, skew, width, height, baseline, and kerning [1]. Ho and Baird compared the OCR accuracy under different values of blur, thresholding, and pixel sensitivity and determined that PSF width and binarization threshold are the two most significant parameters [11]. Figure 1 shows a model of the production of bilevel digitized images using only the PSF and thresholding parameters. Each combination of PSF width,  $w$ , and binarization threshold,  $\Theta$ , produces a different digitized image. The degradations in a scanned image are due to these two

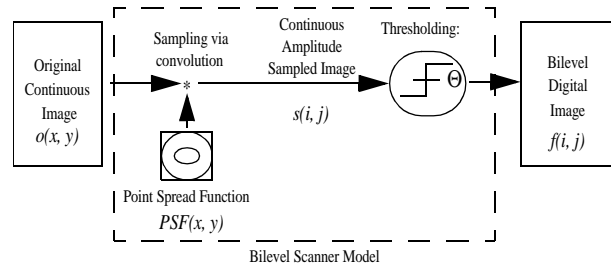


Figure 1: This scanner model is used to determine the value of the pixel  $(i, j)$  centered on each sensor element.

parameters. The degradation type, more than the individual parameter values, is used to describe the image quality.

This paper describes two degradation types. It describes how these degradations are related to the parameters  $w$  and  $\Theta$ . Characters synthetically generated with width and threshold values that produce a common degradation are shown for comparison. Methods for estimating the degradations are briefly discussed, followed by a discussion of when knowledge of the amount of degradation is adequate or when we must go beyond this and estimate values for  $w$  and  $\Theta$  as well.

## 2. Degradation Types

When a character image is degraded, the two most

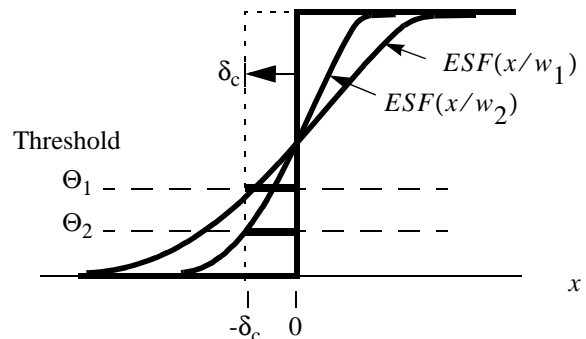


Figure 2: Edge after blurring with a generic PSF of two widths,  $w$ . Two thresholds are shown that produce the same edge shift  $\delta_c$ .

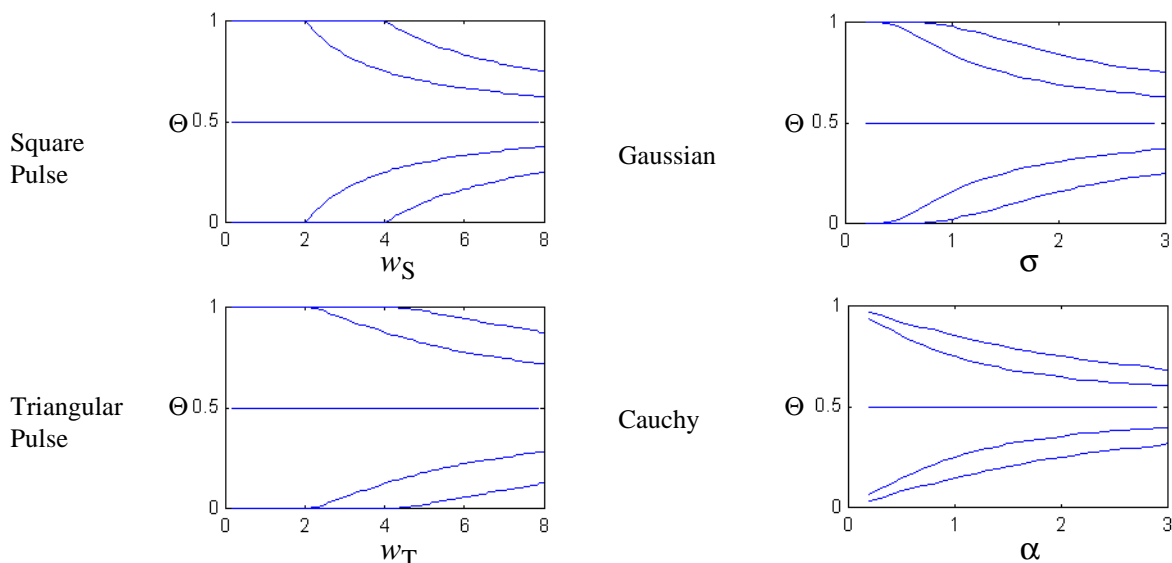


Figure 3: Contours showing constant edge spread of  $\delta_c = [-2 -1 0 1 2]$  (from top to bottom) for four PSF functions.

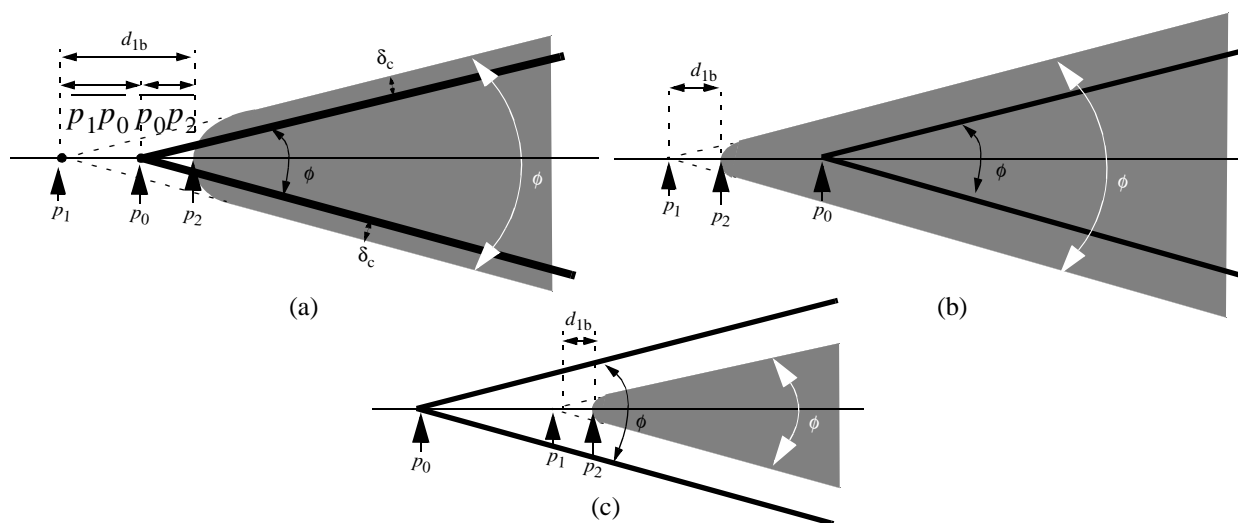


Figure 4: Three possible ways in which a blurred corner (grey area) may be displaced from the original position (black lines).

noticeable effects are a change in the stroke width and a change in the shape of the corners. Both of these degradations are caused by a joint effect of the point spread function width,  $w$ , and the binarization threshold,  $\Theta$ . This relationship can be quantified to describe the amount of the degradation.

## 2.1 Edge Displacement

The stroke width is determined by the location of the edges of the stroke. The stroke width will change as the edge locations move. During scanning, the edge changes from a step to an edge spread function, ESF, through convolution with the PSF. This is then thresholded to reform a step edge, Figure 2. The amount an edge was displaced after scanning,  $\delta_c$ , was shown in [3] to be related to  $w$  and  $\Theta$  by

$$\delta_c = -w \text{ESF}^{-1}(\Theta). \quad (1)$$

The distance that an edge is displaced depends on the threshold, the PSF width and the functional form of the PSF. An infinite number of  $(w, \Theta)$  values could produce any one  $\delta_c$  value. Eq. (1) holds when edges are considered in isolation, for example when the edges are separated by a distance greater than the support of the PSF. Figure 3 shows how the values of  $(w, \Theta)$  vary for 5 different constant  $\delta_c$  values for each of four PSF shapes. A positive threshold value will produce a negative edge displacement. The curves for  $\delta_c$  and  $-\delta_c$  are symmetric around the  $\Theta=1/2$  line. If  $\Theta=1/2$ ,  $\delta_c=0$  for all values of  $w$ .

## 2.2 Corner Erosion

The other major degradation important to bilevel

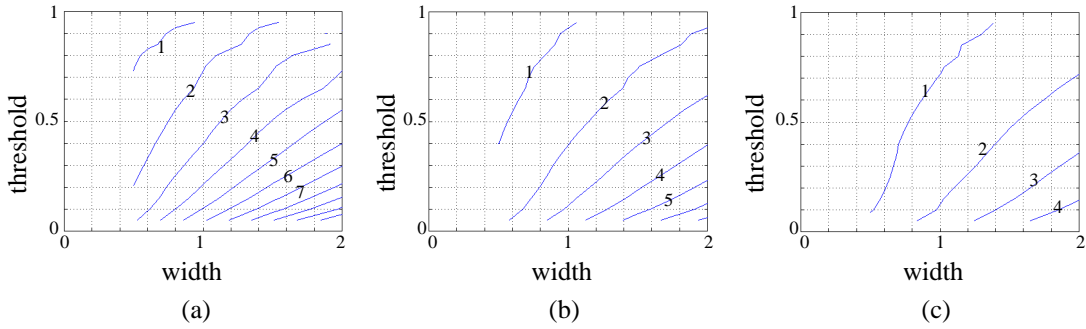


Figure 5: Observable erosion contours for constant  $d_{1b}$  loci for a Gaussian PSF  
(a)  $\phi=\pi/6$  (b)  $\phi=\pi/4$  (c)  $\phi=\pi/3$

images is the shape of a corner [5]. At a distance greater than one half the support of the PSF from the corner, only edge spread effects are present. Nearer to the intersection of the two edges, a degradation is caused by the interaction of the two edges. The degradation of a corner can occur in any of the three forms shown in Figure 4. The point  $p_0$  is the apex of the original corner. The point  $p_2$  is the point along the angle bisector of the new rounded corner where the blurred corner equals the threshold value. The point  $p_1$  is the point where the new corner edges would intersect if extrapolated. The distance that a corner is eroded from the original apex point  $p_0$  depends on the threshold, the PSF width and the functional form similar to the edge displacement above.

One common aspect of these degradations is the amount of the corner that is eroded away, shown as the distances  $\overline{p_0p_2}$  and  $d_1$  in Figure 4. The equation for the amplitude of the blurred corner along its line of symmetry can be written as a function of  $w$  and  $\phi$ ,

$$f_b(d_{0b};w, \phi) = \int_{x=0}^{x=\infty} \int_{y=-x \tan \frac{\phi}{2}}^{y=x \tan \frac{\phi}{2}} PSF(x-d_{0b}, y;w) dy dx, \quad (2)$$

in which case

$$\overline{p_0p_2} = f_b^{-1}(\Theta;w, \phi). \quad (3)$$

Measuring distance  $\overline{p_0p_2}$  requires knowledge of the original location of the corner, which is not easily found on its own.

Further from the corner, the edges do not interfere with each other during blurring and the edge spread effect discussed earlier is present. The distance between point  $p_1$  and point  $p_0$  is a function of edge spread and the corner angle:

$$\overline{p_1p_0} = \frac{\delta_c}{\sin(\phi/2)} = \frac{-wESF^{-1}(\Theta)}{\sin(\phi/2)}. \quad (4)$$

The scanned edges will be parallel to the original edges, allowing the angle  $\phi$  to be measured. The point  $p_1$  and  $p_2$  can be located easily. The distance between points  $p_1$  and  $p_2$  is the sum of the two distances since the points are collinear, therefore

$$\begin{aligned} d_{1b} &= \overline{p_1p_2} = \overline{p_1p_0} + \overline{p_0p_2} \\ &= \frac{-wESF^{-1}(\Theta)}{\sin(\phi/2)} + f_b^{-1}(\Theta;w, \phi) \end{aligned} \quad (5)$$

While this is not the erosion from the original corner location, it does represent the degradation actually seen on the corner. A given amount of corner erosion can also occur for an infinite number of  $(w, \Theta)$  values. Samples of constant  $d_{1b}$  for three angles  $\phi$  are shown in Figure 5.

The three corner erosion cases in Figure 4 are determined by the corner angle and the threshold. They are generally independent of the PSF shape and width,  $w$ . The cases in Figures 4a and b have  $\delta_c > 0$  and thus occur when  $\Theta < 0.5$ . The case in Figure 4b will occur for extremely small values of  $\Theta$ . The erosion case in Figure 4c has an edge displacement of  $\delta_c < 0$  which will occur only when  $\Theta > 0.5$ . As the corner angle  $\phi$  increases, the case in Figure 4b occurs for a larger range of  $\Theta$ .

A white corner on a black background will also be eroded, but in an opposite manner from the black corners. The amount of erosion has the relationship

$$d_{1w} = \frac{-wESF^{-1}(1-\Theta)}{\sin(\phi/2)} + f_b^{-1}(1-\Theta;w, \phi). \quad (6)$$

Samples of this are shown in Figure 6. It can be observed that the contours for black and white corners are symmetric to each other about the  $\Theta=1/2$  line, similar to the relationship between  $\delta_c$  and  $-\delta_c$ .

For both black and white corners, the angle between the edges affects the range of  $d_1$  that will occur for a given PSF width. Larger angles,  $\phi$ , will show less erosion for the same range of  $w$ .

### 3. Sample Characters

These two types of degradation, edge displacement and corner erosion, are present in various combinations for all scanned characters. To illustrate how much each affects characters, 12-point sans-serif font characters  $\theta$ ,  $m$ ,  $x$  and  $z$  are synthetically blurred. The characters are created at 600dpi "scanning" resolution and are shown at twice their standard size. These characters are created with  $(w, \Theta)$  values to give constant edge spread and

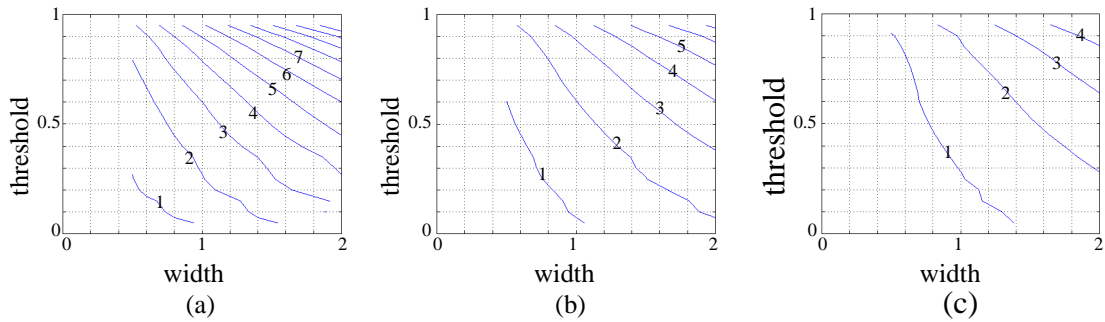


Figure 6: Observable erosion contours for constant  $d_{1w}$  loci for a Gaussian PSF  
(a)  $\phi=\pi/6$  (b)  $\phi=\pi/4$  (c)  $\phi=\pi/3$ .

Edge Displacement:		$\delta_c = -2$	$\delta_c = -1$	$\delta_c = 0$	$\delta_c = 1$	$\delta_c = 2$
Synthetic Characters	Square Pulse	emxZ emxZ emxZ	emxZ emxZ emxZ	emxZ emxZ emxZ	emxZ emxZ emxZ	emxZ emxZ emxZ
	Triangular Pulse	emxZ emxZ emxZ	emxZ emxZ emxZ	emxZ emxZ emxZ	emxZ emxZ emxZ	emxZ emxZ emxZ
	Gaussian	emxZ emxZ emxZ	emxZ emxZ emxZ	emxZ emxZ emxZ	emxZ emxZ emxZ	emxZ emxZ emxZ

Figure 7: Comparison of characters with common  $\delta_c$  values. Three different  $(w, \Theta)$  values produced samples for each PSF. (Note: characters as seen in the proceedings have extra degradation from printing of this paper.)

constant corner erosion. As each of these degradations can occur for multiple thresholds, PSF widths, and functional forms, each of these parameters are varied to show their effects.

### 3.1 Edge Displacement

Five edge spread values, -2, -1, 0, 1 and 2, were shown in Figure 3. Three  $(w, \Theta)$  values were selected for each of these  $\delta_c$  values for three PSF shapes and synthetic characters were generated, Figure 7. The range of the  $(w, \Theta)$  values is large, but the characters appear quite similar due to the constant  $\delta_c$ . Differences can still be seen among characters with a constant  $\delta_c$ , particularly where the lines intersect. This is because the  $\delta_c$  calculation is only valid when the edges are isolated from other edges. Please note that the characters, as seen in the printed proceedings, show additional degradations from the printing of the manuscript and the printing of the proceedings. This also holds for the characters in Figures 8 and 9.

### 3.2 Corner Erosion

For constant corner erosion, the angles present in the characters affect the corner erosion. The locus of  $(w, \Theta)$  points that give constant corner erosion of  $d_1$  for an angle  $\phi_1$  will not give a constant corner erosion for an angle  $\phi_2$ . Figure 8 shows characters created with three  $(w, \Theta)$  values selected to give the corner erosion values of  $d_{1b}=1, 2$  and 3 on the outermost black corners of the letter x. These corners have an approximate measure of 0.95 radians. In Figure 9, the  $(w, \Theta)$  values were chosen to give corner erosions  $d_{1w}=1, 2, 3$  for the white corners in the letter z, which are also approximately 0.95 radians.

The black corners in the x and the white corners in the z have approximately the same angle measure. Therefore the amount of erosion on the black corners of the x and white corners of the z have an inverse relationship. Characters in Figure 9 were created with the same PSF width as the characters in the corresponding locations in Figure 8, but the threshold was  $1-\Theta$ . As the amount of erosion in the black corners increase, some of the white corners increase and some do not. This is because the contours for constant corner erosion in white wedges are

Black Corner Erosion		$d_{1b} = 1$	$d_{1b} = 2$	$d_{1b} = 3$
Synthetic Characters	Square Pulse	emxZ emxZ emxZ	emxZ emxZ emxZ	emxZ emxZ emxZ
	Triangular Pulse	emxZ emxZ emxZ	emxZ emxZ emxZ	emxZ emxZ emxZ
	Gaussian	emxZ emxZ emxZ	emxZ emxZ emxZ	emxZ emxZ emxZ

Figure 8: Comparison of scanned and synthetic characters based on constant  $d_{1b}$  values based on the acute black corners on the tips of the letter x. (Note: characters as seen in the proceedings have extra degradation from printing of this paper.)

White Corner Erosion		$d_{1w} = 1$	$d_{1w} = 2$	$d_{1w} = 3$
Synthetic Characters	Square Pulse	emxZ emxZ emxZ	emxZ emxZ emxZ	emxZ emxZ emxZ
	Triangular Pulse	emxZ emxZ emxZ	emxZ emxZ emxZ	emxZ emxZ emxZ
	Gaussian	emxZ emxZ emxZ	emxZ emxZ emxZ	emxZ emxZ emxZ

Figure 9: Comparison of scanned and synthetic characters based on constant  $d_{1w}$  values based on the acute white corners on the interiors of the letter z. (Note: characters as seen in the proceedings have extra degradation from printing of this paper.)

the at the locations of the black corners flipped about the  $\Theta=1/2$  line. Therefore when following a contour for a black corner erosion, the white corner erosion will grow or shrink depending on the direction one moves along the black contour.

Within the groups of characters with constant corner erosion, some characters' strokes are widened, some are narrowed. This gives the characters a considerable variation in appearance between characters with the same corner erosion, much more than was seen for characters with equal edge spread and varied corner erosion. The feature which people notice most easily is the stroke width. When this is constant, characters appear similar. Characters with constant corner erosion do not usually have the same edge displacement, as can be seen in

Figures 8 and 9.

#### 4. Estimation Methods

While many methods are available to estimate the scanner characteristics from a grey-level scan [6-10,12-15], very little research has been completed on estimating scanner parameters from bilevel scans [2,4]. The scanner calibration methods that use grey-level information either directly or indirectly consider the profile of the blurred edge. Only the location of the edges is available in bilevel images. Bilevel images require new PSF width estimation techniques because the edge profile is no longer available. Here we are concerned with estimating  $\delta_c$  and  $d_1$  more than  $w$  and  $\Theta$ , although knowledge of  $w$  and  $\Theta$  can be used to estimate  $\delta_c$  and  $d_1$  via

Eqs. (1), (5) and (6).

#### 4.1 Edge Displacement

A method of estimating the edge spread was described in [3]. This involved using star sector test charts. The edge spread is related to the number of pixels that are black in annular bands at a given radius relative to the number of pixels that were black in the original star image. If the original star image has bands of equal black and white of width  $\tau(r)$ , then

$$\delta(r) = \left( fr(r) - \frac{1}{2} \right) \tau(r) , \quad (7)$$

where  $fr(r)$  is the fraction of pixels in an annulus at radius  $r$  that are black. If the sector edges are separated by more than the support of the PSF, this amount will be constant,  $\delta_c$ .

The edge displacement can then be estimated by counting the number of black and white pixels at each radius starting at the center of the star. When the quantity  $\delta(r)$  becomes constant,  $\delta_c$  is known.

In practice, this estimation method gives a relatively good estimate of  $\delta_c$ . It is, however, sensitive to the quality of the star chart. If the star chart does not have equal sectors of black and white, the estimate of  $\delta_c$  will not be accurate unless the variation is known and accounted for by modifying the formula. Star charts enable measurement of the edge spread  $\delta_c$ , but star charts aren't available in most documents. In practice, this can be overcome partially by scanning a star chart before a batch of documents. This would not work when this analysis is extended to include multiple bilevel processes in series like the ones occurring when printing then scanning, or photocopying, unless the star chart was present in the original document. Edge displacement could be estimated from other features readily available in documents, such as characters, if the exact stroke width present before scanning is known. It is however, quite unlikely that, for a general document, the exact stroke width of any feature would be known *a priori*.

#### 4.2 Corner Erosion

In [5], a method of estimating the erosion of a corner was presented. This was for the observed erosion and not the erosion from the original corner location. The measure of corner erosion also contained, at least partially, the edge spread estimate.

Measuring the distance between the extrapolated vertex point  $p_1$  and the apex point  $p_2$  will give us the erosion distance,  $d_1$ . The value of  $d_1$  is specific to each corner angle. That angle,  $\phi$ , can be measured from the image.

When  $\phi$  and  $d_{1b}$  are measured from an image, a locus

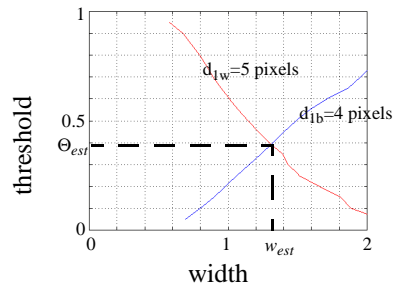


Figure 11: The system parameter estimate is where  $d_{1b}$  and  $d_{1w}$  loci intersect.

of  $(w, \Theta)$  points can be found, like in Figure 5. The  $w$  and  $\Theta$  values depend on the measured erosion distance,  $d_1$ . Small angles will have  $d_1$  contours spaced close together so an error in measuring  $d_1$  will make only a small change in the estimate of  $w$  and  $\Theta$ . Larger angles are much more common in characters than small angles, but the  $d_1$  loci are widely spaced for pairs of  $d_1$  distances that differ by 1 pixel. Thus, an error of 1 pixel caused by noise on the apex pixel or phase effects will greatly affect the estimates for large angles.

When at least one black and one white corner are available, the difference in orientation of the constant erosion  $d_{1b}$  and  $d_{1w}$  loci for black and white corners is utilized to estimate the parameters. The intersection of the  $d_1$  loci from black and white corners should occur at the  $(w, \Theta)$  value for that scanner (Figure 11). This method will still work when  $d_1$  data is collected from black and white corners of different angle measures, increasing the amount of data that can be used on a given page of text or in a given line drawing. Corners are readily available in most images to be used for estimation of the scanner parameters  $w$  and  $\Theta$ .

### 5. Discussion

Two bilevel image degradations were introduced: edge displacement,  $\delta_c$ , and corner erosion,  $d_1$ . These were related to the bilevel process variables PSF width,  $w$ , and binarization threshold,  $\Theta$ . Each of these degradations can be caused by an infinite number of  $w$  and  $\Theta$  values. Corner erosion has a different relationship to  $w$  and  $\Theta$  if the corner is white on a black background as opposed to a black corner on a white background.

These degradations affect how a character looks after scanning. Characters with a constant edge displacement will have a similar look, even for different  $w$  and  $\Theta$  values. Characters with a constant corner erosion will have a different appearance. This can be attributed to character similarity being gauged mostly by the stroke width.

Methods of measuring the amount of edge displacement and corner erosion have been described. Estimation of edge displacement requires a special test pattern, or at least one that is specified in great detail. Estimation of corner erosion requires only knowing that the corner

was originally made by the intersection of two straight lines. Therefore, the estimation of corner erosion is easier on common images and shows great promise for use in document analysis.

Both edge displacement and corner erosion can occur for an infinite set of  $w$  and  $\Theta$  values. When estimating edge spread, it is less critical to estimate both  $w$  and  $\Theta$  to characterize the system for the purpose of generating sample outputs from that system. When estimating the corner erosion, a good estimate of the PSF width and the binarization threshold are needed to generate synthetic characters corresponding to that system. The parameters  $w$  and  $\Theta$  can be estimated by combining the corner erosion estimates from a black and a white corner.

A large number of pixels are used when estimating  $\delta_c$  from star charts. The estimate of  $d_1$  often relies on the value of a single pixel at the tip of the rounded corner to determine the estimate. A large number of corners is needed to get an estimate with the same amount of averaging present in estimates of  $\delta_c$ .

These two degradation parameters have distinctly different characteristics in how they affect an image and how they can be estimated with current techniques. There is a need to integrate the estimation of the two parameters. As corner erosion contains the edge displacement in its calculations, there is potential in continuing research in that direction. Documents usually are subjected to multiple bilevel degradations, so significant advantages will result from expanding this analysis to other bilevel processes such as printing, photocopying and faxing, as well as multiple combinations of these processes.

## 6. Acknowledgement

I would like to thank George Nagy for his useful ideas and comments that encouraged this work.

## 7. References

- [1] Henry S. Baird, "Document Image Defect Models," Proc. IAPR Workshop on Syntactic and Structural Pattern Recognition, Murry Hill, NJ, June 1990, pp. 13-15. Reprinted in H. S. Baird, H. Bunke, and K. Yamamoto (Eds.), *Structured Document Image Analysis*, Springer Verlag: New York, 1992, pp. 546-556.
- [2] Henry S. Baird, "Calibration of document image defect models," *Proc. of Second Annual Symposium on Document Analysis and Information Retrieval*, Las Vegas, Nevada, April 1993, pp. 1-16.
- [3] Elisa H. Barney Smith, "Characterization of Image Degradation Caused by Scanning," *Pattern Recognition Letters*, Volume 19, Number 13, 1998, pp. 1191-1197.
- [4] Elisa H. Barney Smith, *Optical Scanner Characterization Methods Using Bilevel Scans*, Doctoral Thesis, Rensselaer Polytechnic Institute, December, 1998.
- [5] Elisa H. Barney Smith, "Estimating Scanning Characteristics from Corners in Bilevel Images," Proc. SPIE Document Recognition and Retrieval VIII, San Jose, CA, 21-26 January 2001, pp.176-183.
- [6] M. Michael Chang, A. Murat Tekalp, A. Tanju Erdem, "Blur Identification using the Bispectrum," *IEEE Trans. Signal Processing*, Vol. 39, October 1991, pp. 2323-2325.
- [7] F. Chazallet, J. Glasser, "Theoretical bases and measurements of the MTF of integrated image sensors," *Proc. SPIE Image Quality: An Overview*, Vol. 549, Arlington, VA, 9-10 April 1985, pp. 131-144.
- [8] Luigi P. Cordella and George Nagy, "Quantitative Functional Characterization of an Image Digitization System," *6th International Conference on Pattern Recognition*, Munich, Germany, 19-22 October 1982, pp. 535-537.
- [9] D. B. Gennery, "Determination of Optical transfer function by inspection of the frequency domain plot," *Journal of the Optical Society of America*, Vol. 63, No. 12, December 1973, pp. 1571-1577.
- [10] C. A. Glasbey, G. W. Horgan, D. Hitchcock, "A note on the grey-scale response and sampling properties of a desktop scanner," *Pattern Recognition Letters*, Vol. 15, No. 7, 1994, pp. 705-711.
- [11] Tin Kam Ho and Henry S. Baird, "Large-Scale Simulation Studies in Image Pattern Recognition," *IEEE Transactions on Pattern Analysis and Machine Intelligence*, Vol. 19, No. 10, October 1997, pp. 1067-1079.
- [12] S. E. Reichenbach, S. K. Park, R. Narayanswamy, "Characterizing digital image acquisition devices," *Optical Engineering*, Vol. 30, No. 2, March 1991, pp. 170-177.
- [13] R. M. Simonds, "Two-dimensional modulation transfer functions of image scanning systems," *Applied Optics*, Vol. 20, No. 4, February 1981, pp. 619-622.
- [14] P. L. Smith, "New Technique for Estimating the MTF of an Imaging System from its Edge Response," *Applied Optics*, Vol. 11, No. 6, June 1972, pp. 1424-1425.
- [15] H. Wong, "Effect of knife-edge skew on modulation transfer function measurements of charged couple device imagers employing a scanning knife edge," *Optical Engineering*, Vol. 30, No. 9, 1991, pp. 1394-1398.